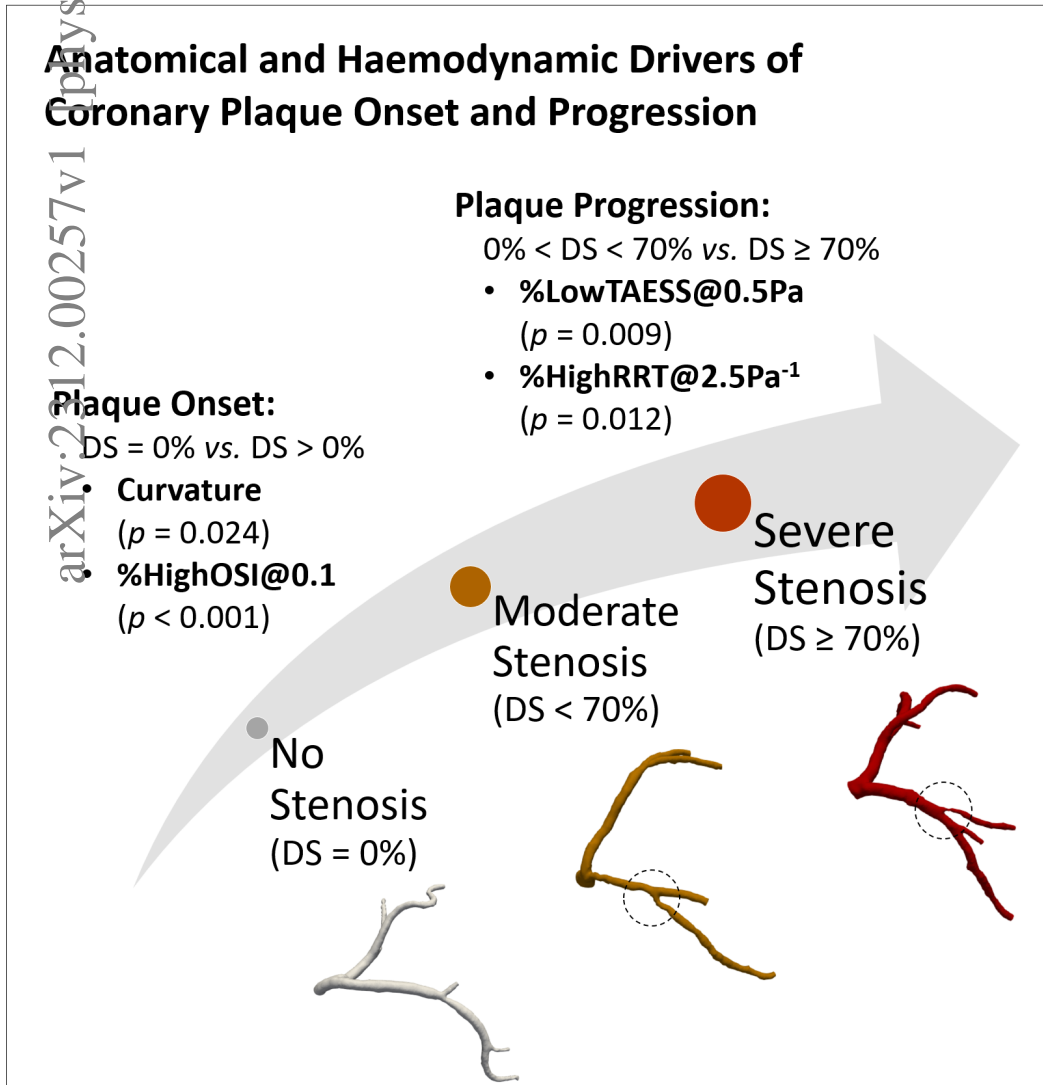


Graphical Abstract

Exploring the Interplay of Left Coronary Tree Anatomy and Haemodynamics: Implications for Plaque Formation

Mingzi Zhang, Ph.D., Ramtin Gharleghi, Ph.D, Chi Shen, M.S., Susann Beier, Ph.D.



Highlights

Exploring the Interplay of Left Coronary Tree Anatomy and Haemodynamics: Implications for Plaque Formation

Mingzi Zhang, Ph.D., Ramtin Gharleghi, Ph.D, Chi Shen, M.S., Susann Beier, Ph.D.

- Vascular curvature and HighOSI appear to be key drivers in the onset of coronary plaque.
- LowTAESS and highRRT may govern plaque progression after onset to severe stenosis.
- Bifurcation-only studies may not be able to capture this mechanism.
- Stenosed bifurcations differ in side branch diameter and distal main vessel torsion.
- Common variations in haemodynamic thresholds did not appear to affect these relationships.

Exploring the Interplay of Left Coronary Tree Anatomy and Haemodynamics: Implications for Plaque Formation

Mingzi Zhang, Ph.D.^{a,*}, Ramtin Gharleghi, Ph.D.^a, Chi Shen, M.S.^a, Susann Beier, Ph.D.^a

^a*School of Mechanical and Manufacturing Engineering, Faculty of Engineering, University of New South Wales, Kensington, NSW 2052, New South Wales, Australia*

Abstract

Background and Objective: The link between atherosclerosis and blood flow-induced haemodynamic luminal shear stresses is well established. However, this understanding has not been translated into clinical practice because of the interdependent effects of the complex coronary anatomy and a multitude of potential haemodynamic metrics, which have been challenging to delineate. Key questions remain, including clarification on the dominant surrogate markers of coronary plaque's focal onset and progression. Thus, this study aims to identify anatomical and haemodynamic differences in coronary trees at different stages of stenoses.

Methods: A total of 39 left coronary trees which are publicly available (ASOCA dataset). Each coronary tree was dissected into bifurcations and non-bifurcating segments for comparisons. We calculated the inflow angle, bifurcation angle, and Finet's ratio for all bifurcations and the average diameter, torsion, and absolute curvature for both non- and bifurcating segments. Transient coronary flow simulations revealed the normalised luminal area exposed to Low Time-Average Endothelial Shear Stress (%LowTAESS), High Oscillatory Shear Index (%HighOSI), and High Relative Residence Time (%HighRRT). We statistically investigated the differences between non-stenosed ($n=20$, Diameter Stenosis $DS=0\%$), moderately ($n=12$, $0\% < DS < 70\%$), and severely ($n=7$, $DS \geq 70\%$) stenosed cases, accounting for multiple comparisons and sample size, after which $p < 0.05^*$ is considered significant.

Results: Only the average curvature and %HighOSI differed between the non-stenosed ($DS=0\%$), and moderately or severely stenosed ($DS > 0\%$) for the coronary trees ($p=0.024^*$ and $p < 0.001^*$), and non-bifurcating segments ($p=0.027^*$ and $p < 0.001^*$), with AUCs of 0.711 and 0.813 for the classification performance. However, the absolute OSI values were comparatively small and should

*Corresponding Author, Ainsworth Building, High St., Sydney, NSW Australia
Phone No: +61 478 899 561
Email address: mingzi.zhang@unsw.edu.au (Mingzi Zhang, Ph.D.)

be interpreted cautiously. %LowTAESS@0.5Pa and %HighRRT@2.5Pa⁻¹ significantly differed between moderately (0%<DS<70%) and severely (DS≥70%) stenosed trees ($p=0.009^*$ and $p=0.012^*$). Classification performance or segment-specific analysis could not be performed due to the sample size ($n<15$).

Conclusions: Our findings suggest curvature and potentially %HighOSI being critical factors in coronary plaque onset in non-bifurcating segments, whereas %LowTAESS and %HighRRT affect plaque progression after onset. This new knowledge may inform future studies and highlight the merit of anatomical and haemodynamic surrogate markers for atherosclerotic risk stratification in coronary artery diseases.

Keywords:

Coronary Artery Disease (CAD), Atherosclerosis, Stenosis, Anatomical Characteristics, Computational Fluid Dynamics (CFD)

1. INTRODUCTION

Coronary Artery Disease (CAD) is a leading cause of morbidity and mortality worldwide. The most common form of CAD is atherosclerotic plaque formations in the epicardial arteries, which may rupture, leading to acute coronary syndrome [1], or become severely obstructive, which limits distal blood supply and causes chronic myocardium ischaemia and death [2]. Therefore, early identification of patients prone to coronary atherosclerosis and their risk stratification may offer opportunities to mitigate the impact and burden of CAD.

It is well established that a patient's age, sex, smoking history, high-density and general cholesterol levels, and blood pressure affect atherogenetic processes. However, there are great variations among individuals in terms of the plaque progression rate [3], and even for confirmed intermediate lesions, the best timing and interventional strategy are still to be explored [4]. Together, nearly 25% of cardiovascular events remain unexplained by our understanding to date [5]. Coronary anatomy and blood flow-induced haemodynamic measures, such as endothelial or wall shear stress (ESS), are considered important factors compounding this residual risk [6]. Yet, delineating which anatomical and haemodynamic metrics, or their combination, would cause plaque development or advance disease stages remains unanswered due to the multi-faceted complexity of the problem.

The low and/or oscillatory shear theory has been the prevalent mechanism attributed to the

focal initiation of atherosclerosis within the cardiovascular system [7]. Thus, a multitude of blood flow metrics have been proposed, including the Time-Averaged Endothelial Shear Stress (TAESS) [8, 9], Oscillatory Shear Index (OSI) [6, 10], Relative Residence Time (RRT) [11], and Wall Shear Stress (WSS) topological skeleton [12, 13].

Since the vascular haemodynamics are imposed by the local arterial anatomy [6], various anatomical features have also been investigated for their efficacy as surrogate markers of pathophysiological phenomena, most notably in clinical literature, coronary tortuosity, best described as average curvature, [14, 15], and more recently, the coronary artery volume index [16] — a ratio of coronary artery volume to myocardial mass, predicting the likelihood of cardiovascular events.

Previous research has anatomically described the whole coronary tree [17]. To our knowledge, there has been limited comprehensive description of the haemodynamics in whole coronary trees however, most studies focused on the bifurcations [17] or stenotic main branches [18] only. Moreover, only a few observations exist on arterial anatomy and haemodynamics before and after plaque onset, wherein the efficacy of WSS and its derivatives in localising plaques was demonstrated [19, 20].

It is also important to note that accurate quantification of coronary anatomy and haemodynamics requires confidence in the image-based reconstruction. In fact, coronary segmentation uncertainty can be as high as 30% [21]. Here, we uniquely use a high-quality dataset [22], comprised of segmentations verified by multiple experts to minimise inter-observer variability.

The aim of this work is to compare the coronary tree anatomy and haemodynamics of symptomatic patients without significant luminal obstruction to patients with lumen-protruding plaques. Using the coronary trees available from the Automated Segmentation Of normal and diseased Coronary Arteries (ASOCA) Challenge [21], we studied non-stenosed, moderately, and severely stenosed cases.

2. METHODS

2.1. *Study Population and Coronary Segmentation*

The open source ASOCA dataset [21] is comprised of 40 CAD cases, of which we excluded one severe case due to extreme stenosis in the Left Anterior Descending (LAD) artery. Of the 39 left main coronary trees studied here, 20 had no significant stenosis, 12 were moderately stenosed, and 7 had severe stenoses.

Table 1: Patient demographics and number of patients in each stenosis category.

Groups	No Stenosis (DS = 0%)	Moderate Stenosis (0%<DS<70%)	Severe Stenosis (DS≥70%)	P-values
Patients	20	12	7	
Female	12/20 (60%)	2/12 (17%)	1/7 (14%)	0.039
Male	8/20 (40%)	10/12 (83%)	6/7 (86%)	0.039
Age	55 ± 8	57 ± 10	59 ± 11	0.328

DS = Diameter Stenosis, p-values were results of Chi-square tests for categorical variables or Welch’s t-tests for continuous variables. Values in the parentheses represent the percentage of the values in the corresponding category.

This dataset is based on Computed Tomography Coronary Angiogram (CTCA) images obtained using a GE LightSpeed 64 slice CT Scanner with an ECG-gated retrospective acquisition protocol. The in-plane resolution of the acquired images was 0.3 to 0.4 mm, and the out-of-plane resolution was 0.625mm [17]. All images were segmented by three experts independently using 3D Slicer [23] before applying an automated majority method to derive the final vascular mask. Refer to Gharlegghi *et al.* [22] for a detailed description of the vascular reconstruction process and **Table 1. 1 (i)** for the patient demographics.

2.2. Computational Model and Boundary Conditions

All distal coronary branches were trimmed if <2 mm in diameter due to the limited resolution of CTCA. Only side branches with diameters >1/3 of the main vessels were preserved. Bifurcating and non-bifurcating coronary tree segments were defined as 10 mm centreline length proximal and distal to the bifurcation point [17] (**Figure 1 [i]**), resulting in 53 bifurcations and 57 non-bifurcating segments for the 20 no-stenosis cases, and 54 bifurcations (12 with stenoses) and 62 non-bifurcating segments (14 with stenoses) for the 19 moderately or severely stenosed cases (**Figure 1 [ii]**). To examine the anatomical and haemodynamic differences by plaque severity, we used a Diameter Stenosis (DS) rate to classify non-stenosed, moderate and severe stenosis with DS=0%, 0%>DS<70%, and DS≥70%, respectively.

Since patient-specific coronary flow conditions were unavailable, we adopted a standard uniform velocity profile and waveform from literature [24] as the inlet condition after scaling according to the patient-specific inlet diameter D , deriving the scaled cycle-averaged flowrate Q [25]:

$$Q = 1.43D^{2.55}. \tag{1}$$

The coronary haemodynamics were quantified assuming a resting state, with a flow split out-flow strategy applied at each bifurcation, dividing the flowrate at the proximal main vessel into

the daughter branches [25]:

$$Q_i = \frac{D_i^{2.27}}{\sum_{k=1}^n D_k^{2.27}} Q_{\text{inflow}}, \quad (2)$$

where n is the number of daughter arteries at a bifurcation, and i refers to the i^{th} daughter branch, D is the diameter averaged from the parameterised centreline points along its 10 mm length, as recommended as appropriate for atherosclerotic arteries where *in vivo* data is unavailable [26], and outflow Q_i is to be calculated.

Computational meshes of each coronary model were generated using ICEM-CFD embedded in the ANSYS package (version 2023R1, Canonsburg, USA), with the maximal sizes of the surface and volume elements determined as 0.1 and 0.2 mm, following a mesh sensitivity analysis. Five prismatic boundary layers adhering to the coronary wall were generated to resolve the near-wall blood flow. The coronary wall was assumed to be rigid, and a laminar fluid model was used with the maximal Reynolds number below 2,000. The blood flow was modelled as incompressible, and the Carreau-Yasuda non-Newtonian fluid model [27] was used to reflect the shear-thinning behaviour of blood.

2.3. Coronary Anatomy and Haemodynamic Analysis

An automated coronary shape analysis was performed on the 3D geometries with the centrelines calculated using an in-house code based on the Vascular Modelling ToolKit (VMTK, version 1.4 [28]). For all non-bifurcating segments and bifurcation branches, *i.e.* the Proximal Main Vessel (PMV), Distal Main Vessel (DMV), and Side Branch (SB), we quantified the average absolute curvature κ_a to quantify vessel tortuosity, as recommended in recent literature [14], following

$$\kappa_a = \frac{1}{L} \int_{s_1}^{s_2} \frac{|\dot{c}'(s) \times \dot{c}''(s)|}{|\dot{c}'(s)|^3} ds, \quad (3)$$

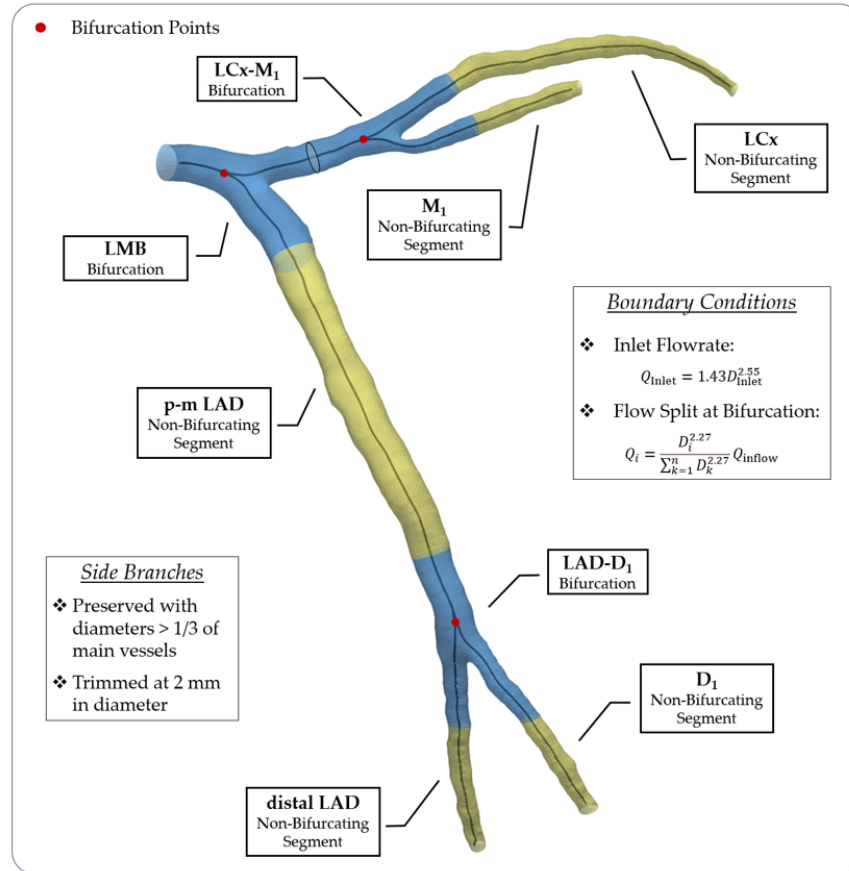
where $c(s)$ denotes the centreline parameterised along the coordinate s of curve c , and L represents the length of a curve considered. Furthermore, we calculated the mean Maximal Inscribed Sphere Diameter (MISD), and torsion τ_a :

$$\tau_a = \frac{1}{L} \int_{s_1}^{s_2} \frac{|(\dot{c}'(s) \times \dot{c}''(s)) \cdot \dot{c}'''(s)|}{|\dot{c}'(s) \times \dot{c}''(s)|^2} ds, \quad (4)$$

For the bifurcations, we additionally computed the inflow angle, bifurcation angle, and the Finet's ratio [17] calculated as

$$\text{FR} = \frac{D_{\text{PMV}}}{D_{\text{DMV}} + D_{\text{SB}}}. \quad (5)$$

(I) Computational settings of a representative coronary tree model, with bifurcating and non-bifurcating segments dissected.



(II) Number of bifurcating and non-bifurcating segments in each stenosis category across the whole tree

Groups	No Stenosis (DS = 0%)	Moderate Stenosis (0% < DS < 70%)		Severe Stenosis (DS ≥ 70%)	
		Stenosis-free	Stenosed	Stenosis-free	Stenosed
<i>Bifurcating Segments</i>					
LMB	20	11	2	8	0
LAD-D1	16	10	4	7	1
LAD-D2	4	5	2	4	2
LCx-M1	13	5	0	4	1
Total	53	31	14	23	4
<i>Non-Bifurcating Segments</i>					
LAD	19	11	2	7	2
LCx	20	12	4	7	1
D1	6	4	1	3	1
LM	3	2	1	1	0
M1	9	8	1	7	1
Total	57	37	9	25	5

DS: Diameter Stenosis.

Fig. 1: Patient demographics and breakdown of the whole left coronary tree into bifurcations (blue) and non-bifurcating (yellow) segments for sub-group analysis with each bifurcation defined as 10 mm along the vascular centreline proximal and distal to the bifurcation point. (LMB: Left Main Bifurcation, LAD: Left Anterior Descending artery, LCx: Left Circumflex artery, D1: the 1st Diagonal artery, M1: the 1st Marginal artery, and p-m LAD indicates the proximal and middle segments of the LAD.)

Table 2: Definitions of coronary geometric parameters for bifurcating and non-bifurcating segments.

Geometric Parameters	Definitions
<i>Non-Bifurcating Segments</i>	
MISD	Mean Diameter of the largest spheres that fit inside the coronary lumen at the points parameterised along the centreline
Aboslute Curvature	Mean κ_a corresponding to the points parameterised along the centreline
Torsion	Mean τ_a corresponding to the points parameterised along the centreline
<i>Bifurcating Segments</i>	
Inflow Angle	Angle with which a PMV enters the bifurcation plane, <i>i.e.</i> , a least-square plane fitted to all the centreline points of the DMV and SB
Bifurcation Angle	Angle of a bifurcation between the DMV and the SB
PMV/DMV/SB Diameter	Mean diameter of the PMV, DMV, or SB
PMV/DMV/SB Curvature	Mean aboslute curvature of the PMV, DMV, or SB
PMV/DMV/SB Torsion	Mean torsion of the PMV, DMV, or SB
Finet's Ratio	Ratio of the mean PMV diameter to that of the mean DMV and SB diameters

PMV: Parent main vessel, DVM: Daughter Main Vessel, SB: Side Branch

A detailed definition of the considered anatomical measures is given in Table. 2.

Transient Computational Fluid Dynamics (CFD) simulations were performed using ANSYS-CFX for four cardiac cycles, with results taken from the fourth cycle to minimise transient start-up effects. A time step of 0.005 seconds was specified for the implicit 2nd order temporal discretisation scheme. The criterion for convergence was set as 10^{-4} for the continuity and normalised velocity and pressure. We quantified the normalised luminal area exposed to adversely low TAESS (%Low-TAESS), high OSI (%HighOSI), and RRT (%HighRRT) due to their association with endothelial cell dysfunction and plaque development [7], calculated as:

$$\text{TAESS} = \frac{1}{T} \int_0^T |\tau_w| dt \quad (6)$$

$$\text{OSI} = \frac{1}{2} \left(1 - \frac{|\int_0^T \tau_w dt|}{\int_0^T |\tau_w| dt} \right) \quad (7)$$

$$\text{RRT} = \frac{1}{(1 - 2 \cdot \text{OSI}) \cdot \text{TAESS}} \quad (8)$$

where τ_w is the flow-induced shear stress vector at the luminal wall, and T denotes the cardiac cycle period.

It is important to note that although low TAESS, high OSI and RRT are generally considered to have an adverse effect on the endothelial cells [?], different thresholds of each parameter have

repeatedly been proposed in the literature with uncertainty around their patho-physiologically relevance. Thus, for comparisons between non-stenosed ($DS = 0\%$) and moderately or severely stenosed ($DS > 0\%$) coronaries, we investigated and reported on all recommended thresholds for %LowTAESS including 0.4, 0.5, 1.3, and 2.5 Pa denoted as, for example, %LowTAESS@0.5Pa [8, 29, 30, 31]. Similarly, for %HighOSI we studied 0.1 and 0.2 [29, 30]. Since RRT is derived from TAESS and OSI, eight thresholds emerged for %HighRRT, *i.e.*, 0.50, 0.67, 0.96, 1.28, 2.50, 3.13, 3.33, and 4.17 Pa^{-1} . We found identical relationships regardless of the threshold chosen as presented in the results (and reported in detail in Appendix A) and thus have not expanded this consideration for the comparisons between moderately ($0\% < DS < 70\%$) and severely ($DS \geq 70\%$) stenosed coronaries, where we instead studied only the most commonly used thresholds, *i.e.*, %LowTAESS@0.5Pa, %HighOSI@0.1, and %HighRRT@2.5 Pa^{-1} .

2.4. Statistical Analysis

The statistical analyses were conducted using the R language-based software JASP (version 0.17.3) [32]. Continuous variables were expressed as mean and Standard Deviation (SD), and categorical variables were given as counts and percentages. Anatomic and haemodynamic differences between the non-, moderately, and severely stenosed arteries were studied for the whole coronary trees, and all bifurcation and non-bifurcating segments. We used a Shapiro-Wilk test to check for the normality of all distributions before using a Welch's t-test for the normally distributed variables or a Mann-Whitney U-test for non-normally distributed variables. Both are considered suitable for the comparison of small samples. To account for the multiple comparisons considered here, we adjusted the p-values with a Bonferroni correction to reduce the chances of a false-positive result (type-I error) before interpreting their significance [33], whereby, after the correction, a $p < 0.05^*$ was considered statistically significant. A Receiver Operating Characteristics (ROC) curve was used to reveal the diagnostic performance if a parameter was significantly different between groups with a minimal sample size > 26 , following a power estimation [?]. The number of patients considered allowed us to only measure the sensitivity, specificity, and area under the ROC curve (AUC) of a parameter in discriminating moderate or severe stenosed arteries ($DS > 0\%$) against non-stenosed arteries ($DS = 0\%$), but not moderately ($0\% < DS < 70\%$) against severely stenosed arteries ($DS \geq 70\%$). Correlations between the anatomical and haemodynamic metrics were examined using the Pearson correlation coefficient r .

3. RESULTS

We found significant differences with coronary trees with different stenosis rates in both coronary anatomy and haemodynamics (**Figure 2**). Only the average absolute curvature and %HighOSI (although with small absolute values) differed between arteries without and with stenosis when comparing the whole trees and non-bifurcating segments ($DS = 0\%$ vs. $DS > 0\%$), whilst the SB diameter and DMV torsion statistically differed between non-stenosed ($DS = 0\%$) and stenosed ($DS > 0\%$) bifurcations. The %LowTAESS and %HighRRT were the only parameters that statistically differed between moderately and severely stenosed arteries ($0\% < DS < 70\%$ vs. $DS \geq 70\%$). Haemodynamic thresholds did not appear to have an effect. Bifurcation-only studies may be misleading as other effects appear to take over with no statistically remarkable findings.

All comparison results are listed in the Appendix, including all considerations of thresholds. Only key comparisons of statistical significance are reported below.

3.1. Plaque onset is affected by coronary curvature and high oscillatory shear stress

Absolute average curvature was the only anatomical characteristic exhibiting a statistically significant difference between the non-stenosed ($DS = 0\%$), and moderately or severely stenosed ($DS > 0\%$) cases when compared for both the whole coronary tree ($DS = 0\%$: 1.230 ± 0.090 vs. $DS > 0\%$: $1.321 \pm 0.131 \text{ m}^{-1}$, $p = 0.024$), and the non-bifurcating segments ($DS = 0\%$: 0.902 ± 0.162 vs. $DS > 0\%$: $1.001 \pm 0.116 \text{ m}^{-1}$, $p = 0.027$), as shown in **Figure 3**). Curvature had a good classification performance in identifying stenosed ($DS > 0\%$) coronary trees, with a sensitivity of 0.842 (95% Confidence Interval [CI]: 0.604 to 0.966), a specificity of 0.600 (95% CI: 0.361 to 0.809), and a AUC of 0.711 (95% CI: 0.543 to 0.844), at the optimal cut-off of 1.227 m^{-1} ($p = 0.015$, **Figure 4**).

However, this held not true for bifurcating segments within the same group classification, *i.e.*, non-stenosed ($DS=0\%$) versus stenosed ($DS > 0\%$) bifurcations ($p > 0.057$). This is most likely attributed to the complex interplay between coronary anatomy and haemodynamics around a bifurcation, which together affect the adverse ESS distribution. However, the SB diameter ($p = 0.041$) and DMV torsion ($p = 0.024$) were statistically different (**Appendix A**), which warrants further analysis to confirm their role in a larger population. Within the anatomical features, coronary curvature negatively correlated with the diameter ($r = -0.474$ and $p = 0.002$), suggesting that smaller arteries tend to be more curved than larger ones.

Similarly, %HighOSI, regardless of the thresholds chosen (@0.1 or @0.2), was statistically different between the non-stenosed coronaries ($DS = 0\%$) and moderately or severely stenosed coronar-

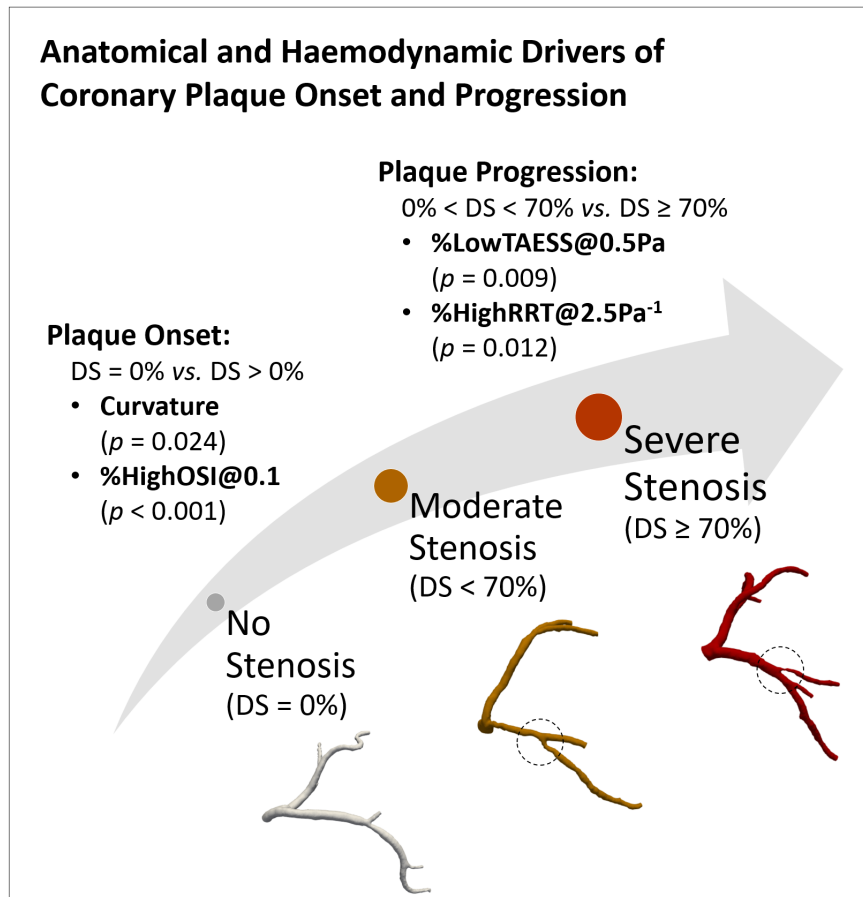


Fig. 2: Comparisons suggest that the average absolute curvature and %HighOSI statistically differed between non-stenosed and moderately or severely stenosed left coronary trees, revealing their link to plaque initiation, whereas %LowTAESS@0.5Pa and %HighRRT@2.5⁻¹ differed between arteries with moderate and severe stenoses, suggesting their role in plaque progression. DS: Diameter Stenosis.

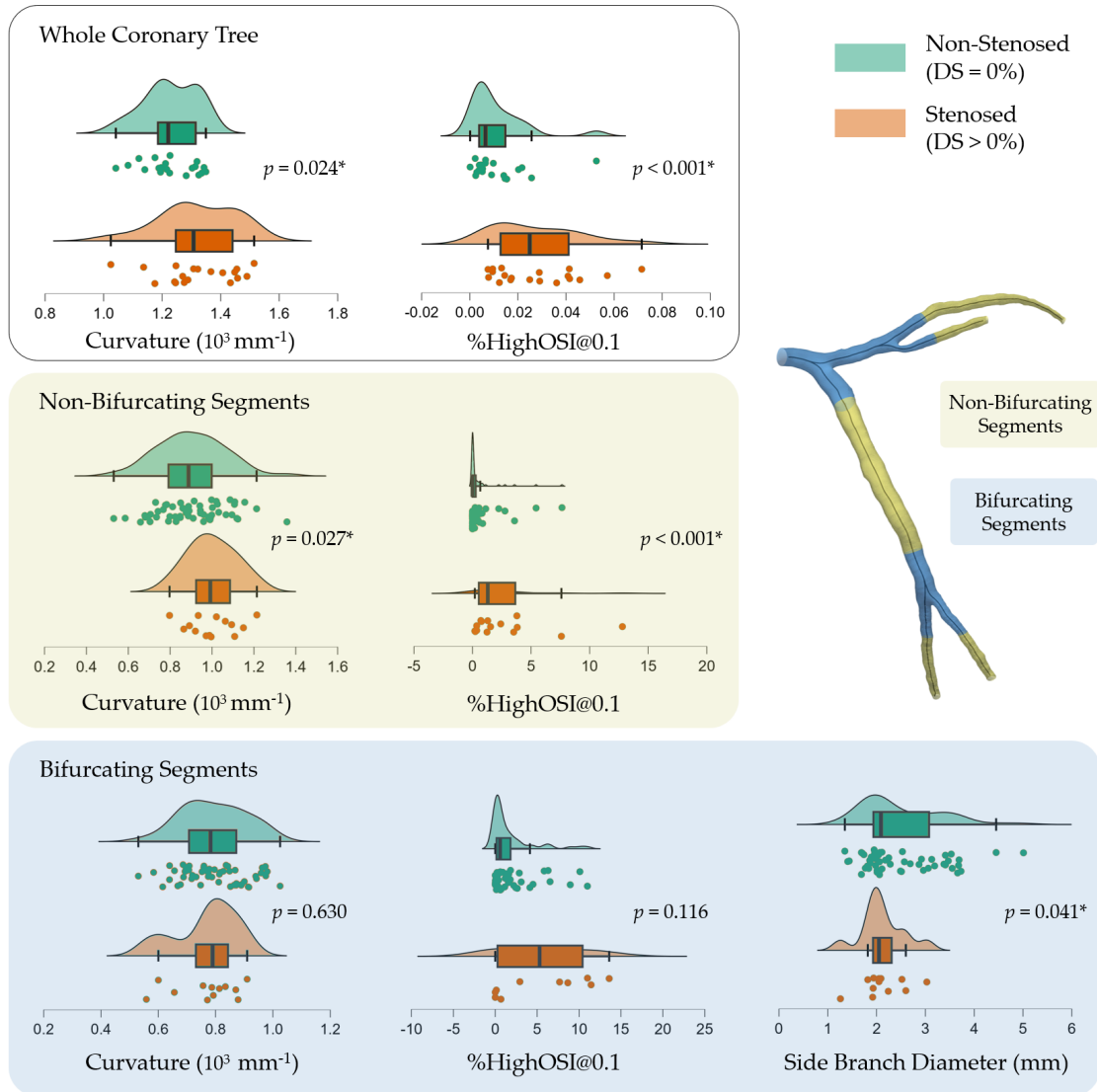


Fig. 3: Comparisons of the whole coronary trees (top: $n=20$ vs. 19), non-bifurcating (middle: $n=57$ vs. 14), and bifurcating segments (bottom: $n=53$ vs. 12) for the differences in the average curvature (left) and %HighOSI — here showing @0.1 threshold for example (right) between patients with no stenosis (DS = 0%) and with moderate or severe stenosis (DS >0%). Differences of statistical significance in the side-branch diameter are also shown for bifurcating segments (bottom-right) and results @0.2 threshold for %HighOSI are provided in the Appendix A.

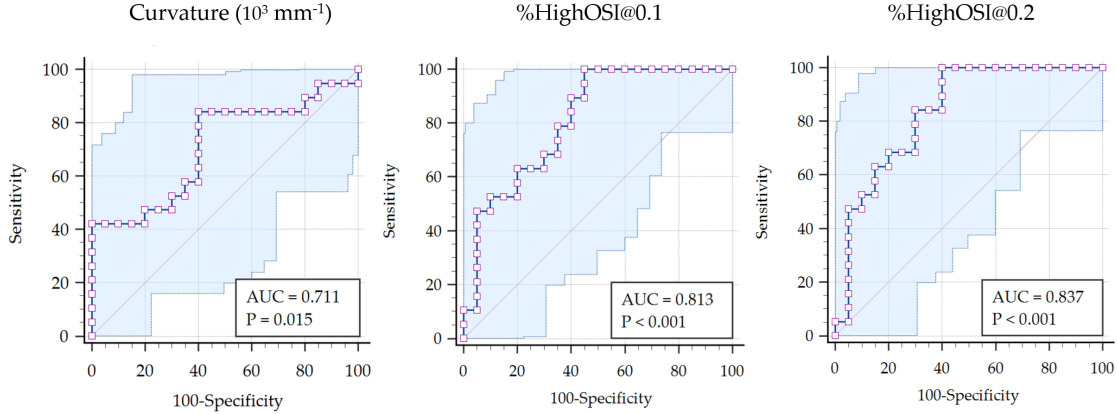


Fig. 4: Diagnostic performance of coronary curvature, %HighOSI@0.1 and %HighOSI@0.2 in differentiating between non-stenosed and moderately or severely stenosed coronary arteries.

ies (DS >70%) , with the former having a lower %HighOSI than the latter for the whole coronary tree (0.011 ± 0.012 vs. 0.028 ± 0.018 , $p < 0.001$) and non-bifurcating segments (0.821 ± 2.004 vs. 2.710 ± 3.438 , $p < 0.001$, **Figure 3**). However, OSI should be interpreted cautiously since the absolute values were generally small (< 0.04 and the luminal area affected by adverse OSI was $< 15\%$). In detecting stenosed (DS >0%) coronary trees, %HighOSI@0.1 had a sensitivity and AUC of 0.999 (95% CI: 0.824 to 0.999) and 0.813 (95% CI: 0.656 to 0.920), and a specificity of 0.550 (95% CI: 0.315 to 0.769) at an optimal cut-off of 0.006 ($p < 0.001$, **Figure 4**). However, for bifurcations only, %HighOSI, irrespective of the thresholds, manifested no statistical difference between non-stenosed and stenosed segments ($p > 0.116$).

3.2. Plaque progression is driven by RRT and TAESS

When comparing moderately ($0 < DS < 70\%$) to severely (DS >70%) stenosed cases only, we found a statistically larger %HighTAESS@0.5Pa (moderate: 0.153 ± 0.135 vs. severe: 0.364 ± 0.130 , $p = 0.009$) and %HighRRT@ 2.5Pa^{-1} (moderate: 0.108 ± 0.095 vs. severe: 0.258 ± 0.118 , $p = 0.012$, **Figure 5**). %HighOSI no longer significantly differed (e.g., @0.1 moderate: 0.026 ± 0.018 , vs. severe: 0.030 ± 0.020 , $p = 0.665$).

Anatomical characteristics, including curvature, did not statistically differ across the coronary tree ($p > 0.272$). Due to the limited sample size within the stenosed groups, *i.e.*, only 4 severely stenosed bifurcations and 5 severely non-bifurcating segments total, a bifurcation-specific or non-bifurcating-segment-specific comparison was not performed.

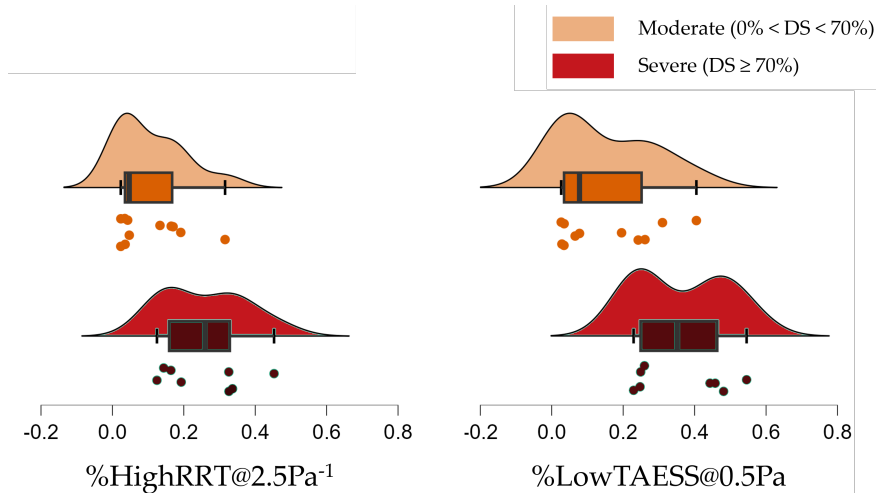


Fig. 5: Differences in $\%HighRRT@2.5Pa^{-1}$ and $\%LowTAESS@2.5Pa$ between moderately ($0\% < DS < 70\%$) and severely ($DS \geq 70\%$) stenosed coronaries.

4. DISCUSSION

We systematically compared differences in the arterial anatomy and blood flow between non-, moderately, and severely stenosed coronaries on the largest publicly available open-source dataset (ASOCA) of CAD patients. Our results revealed the potential shape and flow characteristics that may drive coronary plaque initiation (*i.e.*, coronary curvature and potentially OSI) and progression (*i.e.*, TAESS and RRT). The initial presentation of atherosclerotic plaques is coronary wall thickening towards the outside of the vascular lumen, extensive compensatory remodelling (also known as positive remodelling), which shows no lumen-protruding effects [34]. Hence, early atherosclerosis is not easily detectable from measurement of the luminal dimensions through invasive coronary angiography. For this reason, key factors driving positive remodelling, including potentially coronary arterial shape and its local haemodynamics, are being extensively studied to gain a better understanding of plaque formation risks. Yet, findings are somewhat contradicting to date, with uncertainty around the exact mechanisms between local haemodynamics and atherogenesis.

For vascular anatomical characteristics, their link to plaque onset and progression remains inconclusive. Although various studies have suggested vascular tortuosity [35, 36], its definition has not been consistent, and some metrics, *e.g.*, the tortuosity index, are even incapable of capturing the actual bending of 3D vessels [14]. Clinical studies tend to measure tortuosity on 2D X-ray fluoroscopy images, defining tortuosity by the number of arterial bending with angles over

a certain degree, *e.g.*, 90° [15], or classifying the shape of vessels concerning their 2D projections, *e.g.*, C- or S-shaped [37]. Even for tortuosity calculated by engineers on 3D centrelines, various equations have been used, including notably the tortuosity index [38] and average absolute curvature [39], *etc.* The inconsistencies in measuring tortuosity have thus disabled comprehensive cross-comparison of the findings from different studies. Moreover, tortuosity may also be affected by variations in the coronary diameter [40], suggesting their potentially confounding effects on the local haemodynamics and, therefore, warrants further detailed analysis. Besides these centreline-based anatomical metrics, recent studies tend to test anatomical metrics based on the length or volume of the coronary arteries, *e.g.*, the coronary artery volume index [16], whereby a high prognostic efficacy for cardiovascular events was reported.

Although TAESS and OSI have both been considered drivers of plaque onset [7], here we observed only OSI to be statistically differing between the non-stenosed and stenosed left coronary arteries. For blood flow investigations, OSI and atherosclerosis were first linked in post-mortem human carotid arteries [10], thereafter, the superior correlation of OSI to intimal thickness was confirmed and suggested for coronary arteries as well [11, 41]. However, parallel studies disagreed, or at least found equivalent efficacy in TAESS and OSI — studies performed on patient-specific coronary models with plaque virtually removed suggested that low TAESS predict the most significant number of plaque locations [19]. At the same time, OSI and RRT had fewer false negative predictions [20]. Nonetheless, the merit of this approach is questionable since the arterial anatomy could have altered as a result of disease development, and virtual removal of plaques from stenosed arteries was reported with the potential of under- or overestimating the size of the healthy lumen [7]. In another longitudinal study on human abdominal aortas, early atherosclerotic lesions were found to co-localise with both low TAESS and high OSI [42]. Yet, the reader is advised to exercise caution with interpreting such findings in the context of other vessels because flow regimes, especially for the aorta, are with much greater Reynolds numbers and thus may have distinct flow fields.

Across these haemodynamic parameters, TAESS estimates the temporal average of the ESS magnitudes, whereby OSI characterises the degree of shear stress reversal and RRT identifies regions exposed to both low and oscillatory ESS. Thus, OSI and RRT may more comprehensively reflect the variation of both shear stress magnitude and direction on endothelial cells in a cardiac cycle. Still, this should be interpreted with caution since OSI is normally very low in coronaries, as demonstrated here, compared to that in carotid and aorta. In addition, there is a lack of funda-

mental studies on how OSI or RRT affect endothelial cells compared to ESS, whereby low TAESS, proximal or distal to a focal plaque, has been linked to plaque progression, and high TAESS at the plaque spot promote plaque erosion [18]. Following similar protocols, our identification of the OSI difference before and after plaque onset, and the RRT difference between the moderate ($0 < DS < 70\%$) and severe ($DS \geq 70\%$) stenoses, warrant further observations on large-scale cohorts, although the effects of RRT have just been endorsed by a recent animal experiment [43]. The insignificant differences for bifurcating segments as observed here also warrant further observation to examine the confounding effects from various anatomical and haemodynamic parameters on a larger patient groups. Bearing these uncertainties in mind, for future work, in addition to factors with established links to endothelial dysfunction, it may also aid to include flow characteristics that are known to prevent plaque formation. One such characteristic is the intensity of helical flow [44, 45], which reportedly has protective effects in animal studies [46].

The absence of patient-specific boundary conditions for our flow simulations may be considered a limitation. However, coronary flow measurement is with great uncertainty and not routinely performed in cardiological practice, and thus may not be feasible for analysis and comparison of large retrospective registries. Non-invasive measurement of coronary artery flow relies on transthoracic Doppler echocardiography, whereas the depth and resolution of imaging, obstruction of the bones, *etc.* have constrained its use within the arteries of LM, LAD and PDA. Invasive approaches capable of measuring the side-branch flows include Doppler sonography performed during Intravascular Ultrasound and TIMI Frame Count (TFC) that derives flow velocity from the counts of cine-angiographic frames [47]. Here, we adopted a scaling method ($n = 2.55$) to estimate the left coronary inflow based on the average diameter of the Left Main (LM) artery, which reportedly correlates well with IVUS-obtained flowrates ($r^2 = 0.87$) [25] and is the most common inflow strategy in this scenario. Thus, standardising the inflow assumption using the flow-diameter relation for population groups improves the simulation efficiency and assures physiologically realistic results.

For outflow conditions, a lumped parameter model is usually applied to account for the stenosis-induced flow re-distribution within the epicardial arteries [48]. This approach requires the total myocardial resistance to be derived from the volume of the heart muscle and is commonly used to capture the fractional flow reserve under the hyperaemic condition [49]. To ease the characterisation of flows for a large population, we previously compared the WSS and pressure drop between coronaries with and without stenosis, respectively under the resting and hyperaemic condition

[50]. The results suggested a mild difference in the average WSS and pressure drop across stenosis of different severities, supporting a flow split method to be used at bifurcations under the resting condition.

This study has some limitations. Although we had used the largest open-source CAD dataset, the sample size is still relatively small due to its retrospective and single-centre nature, where the comparisons between small samples were accounted for by using the Welch's *t*-tests rather than the Student *t*-tests. Moreover, we have only included the most used haemodynamic metrics with established links to endothelial dysfunction. However, future work would benefit from including recently proposed novel parameters as well, *e.g.*, the WSS topological skeleton. Finally, we have included only symptomatic patients with no, moderate, or severe stenoses at their first visit, without follow-ups to confirm their longitudinal changes. Virtual removal of plaques from stenosed arteries, as performed in prior studies[19, 20], may enable a pseudo track of the local haemodynamics before plaque onset, whereas the uncertainties introduced in this manual procedure would be challenging to assess. However, we acknowledge the critical importance of longitudinal studies starting from the healthy state to plaque progression to understand better the link of vascular shape and blood flow to CAD trajectory.

5. CONCLUSIONS

Based on anatomic and blood flow analysis on the largest open-source dataset ASOCA, we found that the curvature and %HighOSI statistically differed between coronaries with no stenosis ($DS = 0\%$) and with moderate or severe stenosis ($DS > 0\%$) ($p < 0.001$), and TAESS and RRT between coronaries with moderate ($0 < DS < 70\%$) and severe ($DS \geq 70\%$) stenoses ($p < 0.012$). This suggests that curvature and OSI may predict plaque onset and TAESS and RRT drive the progression of plaques from the moderate to severe stage. Our findings contribute to a clearer understanding of the anatomical and haemodynamic drivers of atherosclerotic plaque initiation and progression, and thus would have direct impact on the prevention, risk prediction and stratification of CAD.

References

- [1] J. F. Bentzon, F. Otsuka, R. Virmani, E. Falk, Mechanisms of plaque formation and rupture, *Circulation Research* 114 (12) (2014) 1852–1866. doi:10.1161/CIRCRESAHA.114.302721.

- [2] P. Xaplanteris, S. Fournier, N. H. Pijls, W. F. Fearon, E. Barbato, P. A. Tonino, T. Engstrøm, S. Käåb, J.-H. Dambrink, G. Rioufol, G. G. Toth, Z. Piroth, N. Witt, O. Fröbert, P. Kala, A. Linke, N. Jagic, M. Mates, K. Mavromatis, H. Samady, A. Irimpen, K. Oldroyd, G. Campo, M. Rothenbühler, P. Jüni, B. De Bruyne, Five-year outcomes with pci guided by fractional flow reserve, *New England Journal of Medicine* 379 (3) (2018) 250–259. doi:10.1056/NEJMoal803538.
- [3] P. Indraratna, E. Khasanova, G. S. Gulsin, G. Tzimas, H. Takagi, K.-H. Park, F. Y. Lin, L. J. Shaw, S.-E. Lee, J. Narula, et al., Plaque progression: Where, why, and how fast? a review of what we have learned from the analysis of patient data from the paradigm registry, *Journal of Cardiovascular Computed Tomography* 16 (4) (2022) 294–302.
- [4] G. Benatti, F. Gragnano, L. Vignali, P. Calabrò, F. L. Gurgoglione, G. Niccoli, Timing and modality of complete revascularization in patients presenting with st-segment elevation myocardial infarction and multivessel coronary artery disease, *International Journal of Cardiology* (2023).
- [5] J. A. Damen, R. Pajouheshnia, P. Heus, K. G. M. Moons, J. B. Reitsma, R. J. P. M. Scholten, L. Hooft, T. P. A. Debray, Performance of the Framingham risk models and pooled cohort equations for predicting 10-year risk of cardiovascular disease: a systematic review and meta-analysis, *BMC Medicine* 17 (1) (2019) 109. doi:10.1186/s12916-019-1340-7.
URL <https://bmcmmedicine.biomedcentral.com/articles/10.1186/s12916-019-1340-7>
- [6] U. Morbiducci, A. M. Kok, B. R. Kwak, P. H. Stone, D. A. Steinman, J. J. Wentzel, Atherosclerosis at arterial bifurcations: evidence for the role of haemodynamics and geometry, *Thrombosis and Haemostasis* 115 (03) (2016) 484–492. doi:10.1160/th15-07-0597.
- [7] V. Peiffer, S. J. Sherwin, P. D. Weinberg, Does low and oscillatory wall shear stress correlate spatially with early atherosclerosis? a systematic review, *Cardiovascular Research* 99 (2) (2013) 242–250, 250 citations (Crossref) [2023-08-29]. doi:10.1093/cvr/cvt044.
- [8] E. M. J. Hartman, G. De Nisco, F. J. H. Gijzen, S.-A. Korteland, A. F. W. Van Der Steen, J. Daemen, J. J. Wentzel, The definition of low wall shear stress and its effect on plaque progression estimation in human coronary arteries, *Scientific Reports* 11 (1) (2021) 22086. doi:10.1038/s41598-021-01232-3.

- [9] Y. Dai, Y. Qian, M. Zhang, Y. Li, P. Lv, X. Tang, A. Javadzadegan, J. Lin, Associations between local haemodynamics and carotid intraplaque haemorrhage with different stenosis severities: A preliminary study based on MRI and CFD, *Journal of Clinical Neuroscience* 66 (2019) 220–225, 4 citations (Crossref) [2023-07-04]. doi:10.1016/j.jocn.2019.05.041.
URL <https://linkinghub.elsevier.com/retrieve/pii/S0967586818314139>
- [10] D. N. Ku, D. P. Giddens, C. K. Zarins, S. Glagov, Pulsatile flow and atherosclerosis in the human carotid bifurcation. positive correlation between plaque location and low oscillating shear stress., *Arteriosclerosis: An Official Journal of the American Heart Association, Inc.* 5 (3) (1985) 293–302, 1771 citations (Crossref) [2022-08-01]. doi:10.1161/01.ATV.5.3.293.
- [11] Y. Hoi, Y.-Q. Zhou, X. Zhang, R. M. Henkelman, D. A. Steinman, Correlation between local hemodynamics and lesion distribution in a novel aortic regurgitation murine model of atherosclerosis, *Annals of Biomedical Engineering* 39 (5) (2011) 1414–1422. doi:10.1007/s10439-011-0255-z.
- [12] U. Morbiducci, V. Mazzi, M. Domanin, G. De Nisco, C. Vergara, D. A. Steinman, D. Gallo, Wall shear stress topological skeleton independently predicts long-term restenosis after carotid bifurcation endarterectomy, *Annals of Biomedical Engineering* 48 (12) (2020) 2936–2949, 17 citations (Crossref) [2023-03-22]. doi:10.1007/s10439-020-02607-9.
- [13] C. Chiastra, V. Mazzi, M. Lodi Rizzini, K. Calò, A. Corti, A. Acquasanta, G. De Nisco, D. Belligiano, E. Cerrato, D. Gallo, U. Morbiducci, Coronary artery stenting affects wall shear stress topological skeleton, *Journal of Biomechanical Engineering* 144 (6) (2022) 061002, 3 citations (Crossref) [2023-03-22]. doi:10.1115/1.4053503.
- [14] V. Kashyap, Accuracy of vascular tortuosity measures using computational modelling, *Scientific Reports* (2022) 10.
- [15] D. Han, A. Lin, K. Kuronuma, E. Tzolos, A. C. Kwan, E. Klein, D. Andreini, J. J. Bax, F. Cademartiri, K. Chinnaiyan, B. J. W. Chow, E. Conte, R. C. Cury, G. Feuchtner, M. Hadamitzky, Y.-J. Kim, J. A. Leipsic, E. Maffei, H. Marques, F. Plank, G. Pontone, T. C. Villines, M. H. Al-Mallah, P. De Araújo Gonçalves, I. Danad, H. Gransar, Y. Lu, J.-H. Lee, S.-E. Lee, L. Baskaran, S. J. Al'Aref, Y. E. Yoon, A. Van Rosendaal, M. J. Budoff, H. Samady, P. H. Stone, R. Virmani, S. Achenbach, J. Narula, H.-J. Chang, J. K. Min, F. Y. Lin, L. J. Shaw, P. J. Slomka, D. Dey,

- D. S. Berman, Association of plaque location and vessel geometry determined by coronary computed tomographic angiography with future acute coronary syndrome–causing culprit lesions, *JAMA Cardiology* 7 (3) (2022) 309. doi:10.1001/jamacardio.2021.5705.
- [16] G. Benetos, R. R. Buechel, M. Gonçalves, D. C. Benz, E. Von Felten, G. P. Rampidis, O. F. Clerc, M. Messerli, A. A. Giannopoulos, C. Gebhard, T. A. Fuchs, A. P. Pazhenkottil, P. A. Kaufmann, C. Gräni, Coronary artery volume index: a novel ccta-derived predictor for cardiovascular events, *The International Journal of Cardiovascular Imaging* 36 (4) (2020) 713–722. doi:10.1007/s10554-019-01750-2.
- [17] P. Medrano-Gracia, J. Ormiston, M. Webster, S. Beier, A. Young, C. Ellis, C. Wang, O. Smedby, B. Cowan, A computational atlas of normal coronary artery anatomy, *EuroIntervention* 12 (7) (2016) 845–854, 29 citations (Crossref) [2022-07-26]. doi:10.4244/EIJV12I7A139.
- [18] P. H. Stone, S. Saito, S. Takahashi, Y. Makita, S. Nakamura, T. Kawasaki, A. Takahashi, T. Katsuki, S. Nakamura, A. Namiki, A. Hirohata, T. Matsumura, S. Yamazaki, H. Yokoi, S. Tanaka, S. Otsuji, F. Yoshimachi, J. Honye, D. Harwood, M. Reitman, A. U. Coskun, M. I. Papafaklis, C. L. Feldman, Prediction of Progression of Coronary Artery Disease and Clinical Outcomes Using Vascular Profiling of Endothelial Shear Stress and Arterial Plaque Characteristics: The PREDICTION Study, *Circulation* 126 (2) (2012) 172–181, 416 citations (Crossref) [2022-04-11]. doi:10.1161/CIRCULATIONAHA.112.096438.
URL <https://www.ahajournals.org/doi/10.1161/CIRCULATIONAHA.112.096438>
- [19] J. Knight, U. Olgac, S. C. Saur, D. Poulidakos, W. Marshall, P. C. Cattin, H. Alkadhi, V. Kurtcuoglu, Choosing the optimal wall shear parameter for the prediction of plaque location—a patient-specific computational study in human right coronary arteries, *Atherosclerosis* 211 (2) (2010) 445–450, 68 citations (Crossref) [2023-08-29]. doi:10.1016/j.atherosclerosis.2010.03.001.
- [20] F. Rikhtegar, J. A. Knight, U. Olgac, S. C. Saur, D. Poulidakos, W. Marshall, P. C. Cattin, H. Alkadhi, V. Kurtcuoglu, Choosing the optimal wall shear parameter for the prediction of plaque location—a patient-specific computational study in human left coronary arteries, *Atherosclerosis* 221 (2) (2012) 432–437. doi:10.1016/j.atherosclerosis.2012.01.018.

- [21] R. Gharleghi, D. Adikari, K. Ellenberger, S.-Y. Ooi, C. Ellis, C.-M. Chen, R. Gao, Y. He, R. Hus-sain, C.-Y. Lee, J. Li, J. Ma, Z. Nie, B. Oliveira, Y. Qi, Y. Skandarani, J. L. Vilaça, X. Wang, S. Yang, A. Sowmya, S. Beier, Automated segmentation of normal and diseased coronary ar-teries – the asoca challenge, *Computerized Medical Imaging and Graphics* 97 (2022) 102049, 0 citations (Crossref) [2022-04-04]. doi:10.1016/j.compmedimag.2022.102049.
- [22] R. Gharleghi, D. Adikari, K. Ellenberger, M. Webster, C. Ellis, A. Sowmya, S. Ooi, S. Beier, Annotated computed tomography coronary angiogram images and associated data of normal and diseased arteries, *Scientific Data* 10 (1) (2023) 128. doi:10.1038/s41597-023-02016-2.
- [23] A. Fedorov, R. Beichel, J. Kalpathy-Cramer, J. Finet, J.-C. Fillion-Robin, S. Pujol, C. Bauer, D. Jennings, F. Fennessy, M. Sonka, J. Buatti, S. Aylward, J. V. Miller, S. Pieper, R. Kikinis, 3d slicer as an image computing platform for the quantitative imaging network, *Magnetic Resonance Imaging* 30 (9) (2012) 1323–1341, 2916 citations (Crossref) [2022-03-28]. doi:10.1016/j.mri.2012.05.001.
- [24] C. Vlachopoulos, M. O’Rourke, W. W. Nichols, McDonald’s blood flow in arteries: theoretical, experimental and clinical principles, CRC press, 2011.
- [25] A. G. van der Giessen, H. C. Groen, P.-A. Doriot, P. J. de Feyter, A. F. van der Steen, F. N. van de Vosse, J. J. Wentzel, F. J. Gijsen, The influence of boundary conditions on wall shear stress distribution in patients specific coronary trees, *Journal of Biomechanics* 44 (6) (2011) 1089–1095, 97 citations (Crossref) [2022-05-01]. doi:10.1016/j.jbiomech.2011.01.036.
- [26] J. T. Schrauwen, J. C. Schwarz, J. J. Wentzel, A. F. van der Steen, M. Siebes, F. J. Gijsen, The impact of scaled boundary conditions on wall shear stress computations in atherosclerotic human coronary bifurcations, *American Journal of Physiology-Heart and Circulatory Physi-ology* 310 (10) (2016) H1304–H1312.
- [27] A. Razavi, E. Shirani, M. Sadeghi, Numerical simulation of blood pulsatile flow in a stenosed carotid artery using different rheological models, *Journal of Biomechanics* 44 (11) (2011) 2021–2030. doi:10.1016/j.jbiomech.2011.04.023.
- [28] L. Antiga, D. A. Steinman, VMTK: vascular modeling toolkit, 2012.

- [29] C. Chiastra, D. Gallo, P. Tasso, F. Iannaccone, F. Migliavacca, J. J. Wentzel, U. Morbiducci, Healthy and diseased coronary bifurcation geometries influence near-wall and intravascular flow: A computational exploration of the hemodynamic risk, *Journal of Biomechanics* 58 (2017) 79–88. doi:10.1016/j.jbiomech.2017.04.016.
- [30] X. Xie, Y. Wang, H. Zhu, J. Zhou, Computation of hemodynamics in tortuous left coronary artery: A morphological parametric study, *Journal of Biomechanical Engineering* 136 (10) (2014) 101006. doi:10.1115/1.4028052.
- [31] P. H. Stone, A. Maehara, A. U. Coskun, C. C. Maynard, M. Zaromytidou, G. Siasos, I. Andreou, D. Fotiadis, K. Stefanou, M. Papafaklis, L. Michalis, A. J. Lansky, G. S. Mintz, P. W. Serruys, C. L. Feldman, G. W. Stone, Role of low endothelial shear stress and plaque characteristics in the prediction of nonculprit major adverse cardiac events, *JACC: Cardiovascular Imaging* 11 (3) (2018) 462–471. doi:10.1016/j.jcmg.2017.01.031.
- [32] J. Team, Jasp (version 0.17.3)[computer software] (2023).
URL <https://jasp-stats.org/>
- [33] O. J. Dunn, Multiple comparisons among means, *Journal of the American Statistical Association* 56 (293) (1961) 52–64. doi:10.1080/01621459.1961.10482090.
- [34] H. Samady, P. Eshtehardi, M. C. McDaniel, J. Suo, S. S. Dhawan, C. Maynard, L. H. Timmins, A. A. Quyyumi, D. P. Giddens, Coronary artery wall shear stress is associated with progression and transformation of atherosclerotic plaque and arterial remodeling in patients with coronary artery disease, *Circulation* 124 (7) (2011) 779–788, 450 citations (Crossref) [2022-03-28]. doi:10.1161/CIRCULATIONAHA.111.021824.
- [35] G. Liu, J. Wu, D. N. Ghista, W. Huang, K. K. Wong, Hemodynamic characterization of transient blood flow in right coronary arteries with varying curvature and side-branch bifurcation angles, *Computers in Biology and Medicine* 64 (2015) 117–126. doi:10.1016/j.combiomed.2015.06.009.
- [36] C. Peng, X. Wang, Z. Xian, X. Liu, W. Huang, P. Xu, J. Wang, The impact of the geometric characteristics on the hemodynamics in the stenotic coronary artery, *PloS One* 11 (6) (2016) e0157490, PMID: 27310014 PMCID: PMC4911169. doi:10.1371/journal.pone.0157490.

- [37] M. S. Altintas, N. Ermis, B. Cuglan, E. Alturk, R. Ozdemir, Influence of right coronary artery shape on timi frame count and lesion distribution, *Archivos De Cardiologia De Mexico* 90 (4) (2020) 475–479, pMID: 33108359. doi:10.24875/ACM.20000083.
- [38] M. Malvè, A. M. Gharib, S. K. Yazdani, G. Finet, M. A. Martínez, R. Pettigrew, J. Ohayon, Tortuosity of coronary bifurcation as a potential local risk factor for atherosclerosis: Cfd steady state study based on in vivo dynamic ct measurements, *Annals of Biomedical Engineering* 43 (1) (2015) 82–93, pMID: 24986333 PMID: PMC7574594. doi:10.1007/s10439-014-1056-y.
- [39] W. E. Hart, M. Goldbaum, B. Côté, P. Kube, M. R. Nelson, Automated measurement of retinal vascular tortuosity, *Proceedings: a conference of the American Medical Informatics Association. AMIA Fall Symposium (1997)* 459–463 PMID: 9357668 PMID: PMC2233372.
- [40] C. Shen, M. Zhang, S. Beier, The effect of diameter variation when accessing patient-specific coronary tortuosity, *Australasian Fluid Mechanics Society (2022)*, Sydney, Australia, 2022, p. Paper No. 241.
- [41] L. Xu, X. Chen, M. Cui, C. Ren, H. Yu, W. Gao, D. Li, W. Zhao, The improvement of the shear stress and oscillatory shear index of coronary arteries during Enhanced External Counterpulsation in patients with coronary heart disease, *PloS One* 15 (3) (2020) e0230144. doi:10.1371/journal.pone.0230144.
- [42] J. Buchanan, C. Kleinstreuer, S. Hyun, G. Truskey, Hemodynamics simulation and identification of susceptible sites of atherosclerotic lesion formation in a model abdominal aorta, *Journal of Biomechanics* 36 (8) (2003) 1185–1196. doi:10.1016/S0021-9290(03)00088-5.
- [43] A. Hoogendoorn, A. M. Kok, E. M. J. Hartman, G. De Nisco, L. Casadonte, C. Chiastra, A. Coenen, S.-A. Korteland, K. Van Der Heiden, F. J. H. Gijzen, D. J. Duncker, A. F. W. Van Der Steen, J. J. Wentzel, Multidirectional wall shear stress promotes advanced coronary plaque development: comparing five shear stress metrics, *Cardiovascular Research* 116 (6) (2020) 1136–1146. doi:10.1093/cvr/cvz212.
URL <https://academic.oup.com/cardiovasres/article/116/6/1136/5553091>
- [44] U. Morbiducci, D. Gallo, S. Cristofanelli, R. Ponzini, M. A. Deriu, G. Rizzo, D. A. Steinman, A

- rational approach to defining principal axes of multidirectional wall shear stress in realistic vascular geometries, with application to the study of the influence of helical flow on wall shear stress directionality in aorta, *Journal of Biomechanics* 48 (6) (2015) 899–906, 54 citations (Crossref) [2022-03-28]. doi:10.1016/j.jbiomech.2015.02.027.
- [45] C. Shen, R. Gharleghi, D. Li, M. Stevens, S. Dokos, S. Beier, Secondary flow in bifurcations – important effects of curvature, bifurcation angle and stents, *Journal of Biomechanics* 129 (2021) 110755, 4 citations (Crossref) [2023-06-11]. doi:10.1016/j.jbiomech.2021.110755.
- [46] G. De Nisco, A. Hoogendoorn, C. Chiastra, D. Gallo, A. M. Kok, U. Morbiducci, J. J. Wentzel, The impact of helical flow on coronary atherosclerotic plaque development, *Atherosclerosis* 300 (2020) 39–46, 28 citations (Crossref) [2023-08-29]. doi:10.1016/j.atherosclerosis.2020.01.027.
URL <https://linkinghub.elsevier.com/retrieve/pii/S002191502030054X>
- [47] V. Kunadian, C. Harrigan, C. Zorkun, A. M. Palmer, K. J. Ogando, L. H. Biller, E. E. Lord, S. P. Williams, M. E. Lew, L. N. Ciaglo, J. L. Buros, S. J. Marble, W. J. Gibson, C. M. Gibson, Use of the timi frame count in the assessment of coronary artery blood flow and microvascular function over the past 15 years, *Journal of Thrombosis and Thrombolysis* 27 (3) (2009) 316–328, PMID: 18425623. doi:10.1007/s11239-008-0220-3.
- [48] C. A. Taylor, T. A. Fonte, J. K. Min, Computational fluid dynamics applied to cardiac computed tomography for noninvasive quantification of fractional flow reserve, *Journal of the American College of Cardiology* 61 (22) (2013) 2233–2241, 692 citations (Crossref) [2022-03-28]. doi:10.1016/j.jacc.2012.11.083.
- [49] H. J. Kim, I. E. Vignon-Clementel, J. S. Coogan, C. A. Figueroa, K. E. Jansen, C. A. Taylor, Patient-specific modeling of blood flow and pressure in human coronary arteries, *Annals of Biomedical Engineering* 38 (10) (2010) 3195–3209, 345 citations (Crossref) [2022-04-30]. doi:10.1007/s10439-010-0083-6.
- [50] M. Zhang, C. Shen, S. Beier, Comparison of two common outflow strategies for resolving coronary haemodynamics under resting and hyperaemic flow conditions., *Australasian Fluid Mechanics Society* (2022), Sydney, Australia, 2022, p. Paper No. 264.

Appendix A. Anatomic and haemodynamic parameters compared at different thresholds

We append four tables of differences in coronary anatomic characteristics (Table A.3) and %LowTAESS (Table A.4), %HighOSI (Table A.5), and %HighRRT (Table A.6) at various thresholds in literature between coronaries without (DS = 70%) and with (DS >70%) stenoses.

Results suggest that Curvature is the only geometrical parameter exhibiting statistically significant difference between non-stenosed (DS = 0%) and moderately or severely stenosed (DS >0%) coronary arteries, and %HighOSI consistently differed between the two groups regardless of the thresholds chosen to determine adverse haemodynamic conditions. However %LowTAESS and %HighRRT consistently manifested no statistically significant differences.

Table A.3: Differences in coronary anatomic characteristics between non-stenosed (DS = 0%) and moderately or severely stenosed (DS >0%) arteries.

Parameters	Groups	N	Mean	SD	SE	P-values
Curvature	Moderate or Severe Stenosis	19	1.321	0.131	0.030	0.024*
	No-Stenosis	20	1.230	0.090	0.020	
Torsion	Moderate or Severe Stenosis	19	4.664	16.715	3.835	0.247
	No-Stenosis	20	-0.322	7.240	1.619	
Diameter	Moderate or Severe Stenosis	19	2.658	0.528	0.122	0.084
	No-Stenosis	20	2.896	0.256	0.058	

N: number of samples; *SD*: standard deviation; *SE*: standard error; and P-values are results of Welch's t-test or Mann-Whitney U-test depending on the distribution of samples.

Table A.4: Differences in %LowTAESS at four common thresholds between non-stenosed (DS = 0%) and moderately or severely stenosed (DS >0%) arteries.

Thresholds	Groups	N	Mean	SD	SE	P-values
%LowTAESS@0.4Pa	Moderate or Severe Stenosis	19	0.157	0.127	0.029	0.901
	No-Stenosis	20	0.174	0.168	0.038	
%LowTAESS@0.5Pa	Moderate or Severe Stenosis	19	0.242	0.168	0.038	0.813
	No-Stenosis	20	0.273	0.184	0.041	
%LowTAESS@1.3Pa	Moderate or Severe Stenosis	19	0.722	0.237	0.054	0.749
	No-Stenosis	20	0.799	0.118	0.026	
%LowTAESS@2.5Pa	Moderate or Severe Stenosis	19	0.906	0.151	0.035	0.204
	No-Stenosis	20	0.961	0.042	0.009	

N: number of samples; *SD*: standard deviation; *SE*: standard error; and P-values are results of Welch's t-test or Mann-Whitney U-test depending on the distribution of samples.

Table A.5: Differences in %HighOSI at two common thresholds between non-stenosed (DS = 0%) and moderately or severely stenosed (DS >0%) arteries.

Thresholds	Groups	N	Mean	SD	SE	P-values
%HighOSI@0.2	Moderate or Severe Stenosis	19	0.013	0.011	0.003	<.001*
	No-Stenosis	20	0.004	0.006	0.001	
%HighOSI@0.1	Moderate or Severe Stenosis	19	0.028	0.018	0.004	<.001*
	No-Stenosis	20	0.011	0.012	0.003	

N: number of samples; *SD*: standard deviation; *SE*: standard error; and P-values are results of Welch's t-test or Mann-Whitney U-test depending on the distribution of samples.

Table A.6: Differences in %HighRRT at eight common thresholds between non-stenosed (DS = 0%) and moderately or severely stenosed (DS >0%) arteries.

Thresholds	Groups	N	Mean	SD	SE	P-values
%HighRRT@0.5Pa ⁻¹	Moderate or Severe Stenosis	19	0.865	0.181	0.041	0.336
	No-Stenosis	20	0.929	0.064	0.014	
%HighRRT@0.67Pa ⁻¹	Moderate or Severe Stenosis	19	0.78	0.216	0.049	0.667
	No-Stenosis	20	0.855	0.099	0.022	
%HighRRT@0.96Pa ⁻¹	Moderate or Severe Stenosis	19	0.631	0.25	0.057	0.901
	No-Stenosis	20	0.699	0.147	0.033	
%HighRRT@1.28Pa ⁻¹	Moderate or Severe Stenosis	19	0.482	0.239	0.055	0.857
	No-Stenosis	20	0.537	0.181	0.041	
%HighRRT@2.5Pa ⁻¹	Moderate or Severe Stenosis	19	0.171	0.128	0.029	0.728
	No-Stenosis	20	0.188	0.166	0.037	
%HighRRT@3.13Pa ⁻¹	Moderate or Severe Stenosis	19	0.107	0.088	0.02	0.807
	No-Stenosis	20	0.117	0.144	0.032	
%HighRRT@3.33Pa ⁻¹	Moderate or Severe Stenosis	19	0.093	0.077	0.018	0.857
	No-Stenosis	20	0.102	0.136	0.03	
%HighRRT@4.17Pa ⁻¹	Moderate or Severe Stenosis	19	0.056	0.048	0.011	0.428
	No-Stenosis	20	0.06	0.095	0.021	

N: number of samples; *SD*: standard deviation; *SE*: standard error; and P-values are results of Welch's t-test or Mann-Whitney U-test depending on the distribution of samples.

Appendix B. Comparisons of the dissected coronary bifurcations and non-bifurcating segments for differences in the anatomic and haemodynamic characteristics

We append two tables for the differences in the bifurcating (Table B.7) and non-bifurcating (Table B.8) segments in terms of the coronary anatomic characteristics and % wall areas exposed to adverse haemodynamics at the most used thresholds, *i.e.*, 0.5 Pa for low TAESS, 0.1 for OSI, and 2.5 Pa⁻¹ for RRT.

Within the blood flow parameters, %LowTAESS and %HighRRT were generally positively correlated across different thresholds ($n = 39$, all $p < 0.002$, with the maximal $r = 0.977$), in contrast to the correlation between %LowTAESS and %HighOSI, with the strongest negative correlation observed between %HighOSI@0.1 *vs.* %LowTAESS@2.5Pa ($r = -0.413$, $p = 0.009$). No other flow parameters showed significant differences when compared between the dissected bifurcating or non-bifurcating segments, irrespective of the thresholds chosen, including %LowTAESS and %HighRRT.

Table B.7: Comparison of coronary shape and haemodynamics between non-stenosed (DS = 0%) and moderately or severely stenosed (DS >0%) bifurcations.

Parameters	Groups	N	Mean	SD	SE	P-values
Anatomical Characteristics						
IA	Moderate or Severe Stenosis	12	161.583	8.273	2.388	0.058
	No-Stenosis	53	155.786	12.297	1.643	
BA	Moderate or Severe Stenosis	12	57.083	28.125	8.119	0.742
	No-Stenosis	53	59.964	20.657	2.760	
PMV diameter	Moderate or Severe Stenosis	12	3.380	0.796	0.230	0.312
	No-Stenosis	53	3.638	0.654	0.087	
DMV diameter	Moderate or Severe Stenosis	12	2.942	0.586	0.169	0.424
	No-Stenosis	53	3.103	0.754	0.101	
SB diameter	Moderate or Severe Stenosis	12	2.121	0.445	0.129	0.041*
	No-Stenosis	53	2.479	0.811	0.108	
FR	Moderate or Severe Stenosis	12	0.678	0.160	0.046	0.851
	No-Stenosis	53	0.669	0.097	0.013	
PMV curvature	Moderate or Severe Stenosis	12	0.677	0.198	0.028	0.630
	No-Stenosis	53	0.668	0.264	0.041	
DMV curvature	Moderate or Severe Stenosis	12	0.775	0.174	0.024	0.995
	No-Stenosis	53	0.769	0.222	0.032	
SB curvature	Moderate or Severe Stenosis	12	0.914	0.286	0.039	0.057
	No-Stenosis	53	0.980	0.316	0.047	
PMV torsion	Moderate or Severe Stenosis	12	3.073	1.302	0.190	0.065
	No-Stenosis	53	2.674	1.892	0.299	
DMV torsion	Moderate or Severe Stenosis	12	3.428	1.567	0.215	0.024*
	No-Stenosis	53	2.771	1.234	0.176	
SD torsion	Moderate or Severe Stenosis	12	3.207	1.248	0.173	0.057
	No-Stenosis	53	2.760	1.083	0.161	
Blood Flow Characteristics						
%LowTAESS@0.5Pa	Moderate or Severe Stenosis	12	22.400	18.650	5.898	0.700
	No-Stenosis	53	26.627	20.983	2.882	
%HighOSI@0.1	Moderate or Severe Stenosis	12	5.614	5.426	1.716	0.116
	No-Stenosis	53	1.714	2.630	0.361	
%HighRRT@2.5Pa ⁻¹)	Moderate or Severe Stenosis	12	20.679	17.353	5.487	0.903
	No-Stenosis	53	22.446	20.770	2.853	

N: number of samples; *SD*: standard deviation; *SE*: standard error; and P-values are results of Welch's *t*-test or Mann-Whitney *U*-test depending on the distribution of samples. IA: inflow angle; BA: bifurcation angle; PMV: proximal main vessel diameter; DMV: distal main vessel diameter; SB: side-branch diameter; and FR: Finet's ratio.

Table B.8: Comparison of coronary shape and haemodynamics between moderate or severe ($DS = 0\%$) and stenosed ($DS > 0\%$) non-bifurcating segments.

Parameters	Groups	N	Mean	SD	SE	P-values
Anatomical Characteristics						
Curvature	Moderate or Severe Stenosis	14	1.001	0.116	0.031	0.027*
	No-Stenosis	57	0.902	0.162	0.021	
Torsion	Moderate or Severe Stenosis	14	3.095	0.681	0.182	0.072
	No-Stenosis	57	3.509	0.717	0.095	
Diameter	Moderate or Severe Stenosis	14	2.594	0.348	0.148	0.303
	No-Stenosis	57	2.686	0.284	0.064	
Blood Flow Characteristics						
%LowTAESS@0.5Pa	Moderate or Severe Stenosis	14	15.180	18.447	1.792	0.129
	No-Stenosis	57	20.968	18.669	4.820	
%HighOSI@0.1	Moderate or Severe Stenosis	14	0.821	2.004	0.195	<.001*
	No-Stenosis	57	2.710	3.438	0.888	
%HighRRT@2.5Pa ⁻¹)	Moderate or Severe Stenosis	14	12.825	17.369	1.687	0.102
	No-Stenosis	57	18.103	17.750	4.583	

N: number of samples; *SD*: standard deviation; *SE*: standard error; and P-values are results of Welch's *t*-test or Mann-Whitney *U*-test depending on the distribution of samples. Tortuosities are the average absolute curvatures derived from the centrelines of each coronary tree.